

Article

Two-Step Magnetic Ordering in Intercalated Niobium Dichalcogenide Mn_XNbS_2

Fedor Mushenok ¹, Artem Shevchun ^{2,3,*}, Dmitriy Shovkun ^{2,3} and Maria Prokudina ²¹ School of Physics, University of Exeter, Exeter EX4 4QL, UK² Osipyan Institute of Solid State Physics RAS, 142432 Chernogolovka, Russia³ Faculty of Physics, HSE University, 101000 Moscow, Russia

* Correspondence: shevchun@issp.ac.ru

Abstract: Transition metal dichalcogenides are studied due to the possibility of creating nanoscale semiconductor devices, as well as fundamental issues of magnetic ordering. We researched the crystal structure and magnetic properties of niobium dichalcogenide $Mn_{0.30}NbS_2$. The results of the X-ray study showed the possible existence of an intermediate $2\sqrt{3}a_0 \cdot 2\sqrt{3}a_0$ structure between the “basic” superstructures. Also, two local maximums were found in the temperature dependence of the dynamic magnetic susceptibility. These features can indirectly confirm the presence of a transition superstructure and reflect the two-step nature of the magnetic ordering.

Keywords: transition metal dynamic susceptibility; magnetic ordering; dichalcogenide

1. Introduction

Transition metal dichalcogenides TX_2 (where $T = Mo, Nb, Ta, Ti, W$; $X = S, Se, Te$) have been relevant objects of study of solid-state physics for several decades. Today, the primary interest in these compounds is due to the discovery of monolayers of TX_2 . Technologies for assembling van der Waals heterostructures have led to the creation semiconductor nanodevices based on individual monolayers of TX_2 : nanoscale field effect transistors [1–4], low-dimensional rectifying contacts [5], phototransistor devices [6], spin-valley filters [7], battery applications [8,9], and photoluminescence effects [10,11].

At the same time, intercalated transition metal dichalcogenides provide a unique opportunity to study the fundamental regularities of magnetic ordering. Transition metal ions intercalated in an initially diamagnetic matrix of TX_2 can form a magnetically ordered structure. The type and temperature of magnetic ordering depend on the concentration of intercalated ions and their valence and spin states, as well as the initial diamagnetic matrix. When tracking the dependence of the type and parameters of magnetic ordering on these parameters, one can find out some regularities that reflect the fundamental properties of magnetic ordering and its relationship with an electron structure. For example, with an increase in the number n of d-electrons, in a series of $M_{1/3}NbS_2$ compounds (where $M =$ transition 3d metal) the transition from a paramagnet ($M = Ti, n = 1$) to a ferromagnet ($M = V, n = 2$) to a helimagnet ($M = Cr, Mn, n = 3–4$) to an antiferromagnet ($M = Fe, Co, Ni, n = 5–7$) is observed.

In an $M_{1/3}NbS_2$ series, $Cr_{1/3}NbS_2$ [12–16] and $Mn_{1/3}NbS_2$ [17–19] are two of the most interesting compounds for the physics of magnetism: a uniaxial helicoidal magnetic structure with the wave vector q directed along the hexagonal axis c is formed in them as a result of competition between symmetric and anti-symmetric exchange interactions. Despite a large number of works devoted to these compounds, the most important crystallographic and magnetic characteristics (the temperature of magnetic ordering, the critical fields of magnetic phase transitions, etc.) obtained by various authors differ significantly. Possible reasons for these differences may be the uncontrolled deviations of chemical composition from the stated one or the non-uniform distribution of intercalated ions in an initial matrix.



Citation: Mushenok, F.; Shevchun, A.; Shovkun, D.; Prokudina, M. Two-Step Magnetic Ordering in Intercalated Niobium Dichalcogenide Mn_XNbS_2 . *Magnetism* **2023**, *3*, 259–266. <https://doi.org/10.3390/magnetism3030020>

Received: 2 April 2023

Revised: 6 July 2023

Accepted: 22 August 2023

Published: 4 September 2023



Copyright: © 2023 by the authors. Licensee MDPI, Basel, Switzerland. This article is an open access article distributed under the terms and conditions of the Creative Commons Attribution (CC BY) license (<https://creativecommons.org/licenses/by/4.0/>).

It was shown in [20] that in $\text{Cr}_{1/3}\text{NbS}_2$ helimagnet, a decrease in the Cr concentration led to an increase in the structural disordering of intercalated ions. This caused a decrease in the temperature of magnetic ordering, as well as the formation of a ferromagnetic not helicoidal magnetic structure. It was shown in [21] that in a single Fe_xTaS_2 crystal, the extreme value of the magnetoresistance corresponds to $x = 0.3$. The present work aimed to study the peculiarities of crystal and magnetic structures in Mn_xNbS_2 when the concentration of intercalated ions x was less than 0.33. It can be seen that this issue is of interest in the scientific community, so this year an article [22] was published on a similar topic.

2. Preparation of Samples and Experimental Methods of Study

Single-crystal $\text{Mn}_{0.30}\text{NbS}_2$ samples were prepared in two stages [23].

In the first stage, the powders of initial chemical elements (Nb, S, and Mn) taken in the required ratio were thoroughly mixed and sealed in an evacuated quartz ampoule. Then, the ampoule was slowly ($5\text{ }^\circ\text{C/h}$) heated to $800\text{ }^\circ\text{C}$ and subjected to this temperature for 14 days, after which the polycrystalline $\text{Mn}_{0.30}\text{NbS}_2$ sample was obtained.

In the second stage, $\text{Mn}_{0.30}\text{NbS}_2$ single crystals were obtained using the method of chemical transport. Iodine with a volume concentration of 5 mg/cm^3 was used as a transport agent. The 25 cm long sealed quartz ampoule with weighed portions of iodine and the polycrystalline $\text{Mn}_{0.30}\text{NbS}_2$ sample obtained in the first synthesis stage was placed in a two-zone tube furnace with independent temperature control in each zone. During the growth, a constant temperature gradient $T = 900\text{--}800\text{ }^\circ\text{C}$ was maintained in the furnace. The weighed portion of the polycrystalline sample was in the zone with a higher temperature. After one week, the furnace was smoothly cooled down to room temperature at a rate of $10\text{ }^\circ\text{C/h}$. In the zone with a reduced temperature, non-transparent single crystals with the shape of thin hexagonal plates or pyramids were found on the walls of the quartz ampoule.

Four selected crystals with regular hexagonal faceting were cleaved along the basal plane into several thin plates. One plate of each crystal was used to determine the chemical composition using energy-dispersive X-ray spectroscopy. Three to five tests were conducted for each plate, and the chemical composition of the obtained crystals was determined, which was $\text{Mn}_{0.30 \pm 0.05}\text{Nb}_{1.08 \pm 0.03}\text{S}_{1.96 \pm 0.05}$.

The polycrystalline $\text{Mn}_{0.30}\text{NbS}_2$ samples and powdered single crystals were tested at room temperature by X-ray diffraction using an ARL X'TRA powder diffractometer, after the first stage and second stage, respectively. The obtained diffraction spectra were compared to the data of the online crystallographic database AtomWork [24].

The crystal structure of the single crystals grown was investigated using a P4 BRUKER single-crystal X-ray diffractometer ($\text{Cu K}\alpha$, $\lambda = 0.154\text{ nm}$).

To determine the magnetic properties of the crystals, the dynamic magnetic susceptibility χ was measured at a frequency of 100 kHz in the temperature range of $T = 5\text{--}300\text{ K}$. A sample was placed inside a pair of coaxial coils with a 6 mm in diameter. One of the coils served to excite an alternating magnetic field, while the other one was used for the measurement [25]. An identical pair of coils used to compensate for a signal in the absence of a sample was put nearby. By using a standard circuit of synchronous detection, we measured the imbalance signal. This signal was proportional to the magnetic moment $M = \chi V H_{ff}$. Here $H_{ff} \approx 0.1\text{ Oe}$ is the amplitude of an alternating magnetic field produced by a coil, and V is the volume of a sample. In addition, we could put a sample in a constant magnetic field H , which had an amplitude of up to 150 Oe and was parallel to a high-frequency field.

3. Structural Studies

The crystal structure of intercalated Mn_xNbS_2 ($x = 0\text{--}0.33$) dichalcogenides is formed by 2D NbS_2 layers that consist of trigonal prisms. S atoms are located at the apexes of the prisms, and Nb atoms are located in the center of every second prism. Intercalated Mn ions take octahedral positions between two adjacent 2D layers. At certain concentrations, x , intercalated ions take ordered positions in the basal plane and form a crystal superstructure [26,27]. For example, at $x = 1/4$ a crystal superstructure of the $2a_0 \cdot 2a_0$ type

with a space group $P6_3/m$ (where $a_0 = 3.3 \text{ \AA}$ is the spacing of the lattice cell of initial non-intercalated NbS_2) is formed. At the concentration $x = 1/3$, intercalated ions form a crystal superstructure of the $\sqrt{3}a_0 \cdot \sqrt{3}a_0$ type with a space group $P6_322$ (see Table 1). Note that the crystallographic parameters of the compounds under study available in the literature often differ by several tenths of \AA . Therefore, the accuracy of the estimations and comparisons provided in this work cannot exceed $0.2\text{--}0.3 \text{ \AA}$.

Table 1. Comparison of the crystallographic data and magnetic properties of Mn_xNbS_2 .

x	$a, b \text{ (\AA)}$	$c \text{ (\AA)}$	Space Group	Type of the Superstructure	$T_C, \text{ K}$
0.25	6.64–6.92	12.46–12.90	$P6_3/m$	$2a_0 \cdot 2a_0$	100
0.30	11.53	12.50	$P\text{-}3m1$	$2\sqrt{3}a_0 \cdot 2\sqrt{3}a_0$	100; 40
0.33	5.78–5.81	12.55–12.64	$P6_322$	$\sqrt{3}a_0 \cdot \sqrt{3}a_0$	40

A change in the concentration of intercalated ions affects both the crystal structure and the type of magnetic ordering. Thus, for $\text{Mn}_{0.25}\text{NbS}_2$ compounds magnetic ordering occurs at $T = 100 \text{ K}$ with the formation of an “easy-plane” ferromagnetic structure [27,28]. At the same time, in $\text{Mn}_{0.33}\text{NbS}_2$ a helicoidal incommensurate magnetic structure [17] with a period of 700 nm and a wave vector directed along the crystallographic axis c is formed at $T = 40 \text{ K}$.

The X-ray powder diffraction spectrum of our $\text{Mn}_{0.30}\text{NbS}_2$ sample was compared to the spectra of $\text{Mn}_{0.33}\text{NbS}_2$ and $\text{Mn}_{0.25}\text{NbS}_2$ [24,26,27,29–33] (Figure 1). For all three compared compounds, the positions of the most intense peaks corresponding to scattering on the atoms of an initial NbS_2 matrix are almost identical. At the same time, the positions of some low-intensity peaks in the spectrum of $\text{Mn}_{0.30}\text{NbS}_2$ cannot be related to any of the reflections of $\text{Mn}_{0.33}\text{NbS}_2$ or $\text{Mn}_{0.25}\text{NbS}_2$ structures. These reflections are marked with arrows in Figure 1. The compounds under discussion differ in the concentration x of intercalated Mn ions, which has little effect on the position of atoms in an initial NbS_2 matrix. Therefore, it is reasonable to assume that the presence of additional peaks in the X-ray diffraction spectrum is due to the difference in the ordering of intercalated Mn ions in the basal plane.

To prove this assumption, single-crystal X-ray diffraction studies were carried out on individual plates cleaved from the selected single crystals. The following parameters of the crystal structure were obtained: $a = b = 11.53 \text{ \AA}$, $c = 12.50 \text{ \AA}$, $\alpha = \beta = 90^\circ$, $\gamma = 120^\circ$, space group $P\text{-}3m1$. The spacing c of the crystal lattice along the hexagonal axis has an intermediate value between the values of this parameter for $\text{Mn}_{0.33}\text{NbS}_2$ and $\text{Mn}_{0.25}\text{NbS}_2$. This agrees well with the previously known dependence of interlayer distance on the concentration of intercalated ions [27]. At the same time, the spacing of a crystal structure in the basal plane $a = b = 11.53 \text{ \AA}$ is much greater than that for $\text{Mn}_{0.33}\text{NbS}_2$ ($\sqrt{3}a_0 = 5.72 \text{ \AA}$) and $\text{Mn}_{0.25}\text{NbS}_2$ ($2a_0 = 6.6 \text{ \AA}$).

The discovered increase in the parameters a, b is most likely due to the formation of a new type of ordering of intercalated Mn ions, which differs drastically from the previously known $2a_0 \cdot 2a_0$ and $\sqrt{3}a_0 \cdot \sqrt{3}a_0$ superstructures. Our value of a, b is close with good accuracy to the value $2\sqrt{3}a_0 = 11.43 \text{ \AA}$, corresponding to the crystal $2\sqrt{3}a_0 \cdot 2\sqrt{3}a_0$ superstructure. This type of superstructure was found earlier under the absorption of Sn atoms on the Si(111) surface [34]. The typical characteristics and conditions for the formation of this type of crystal structure have to be studied.

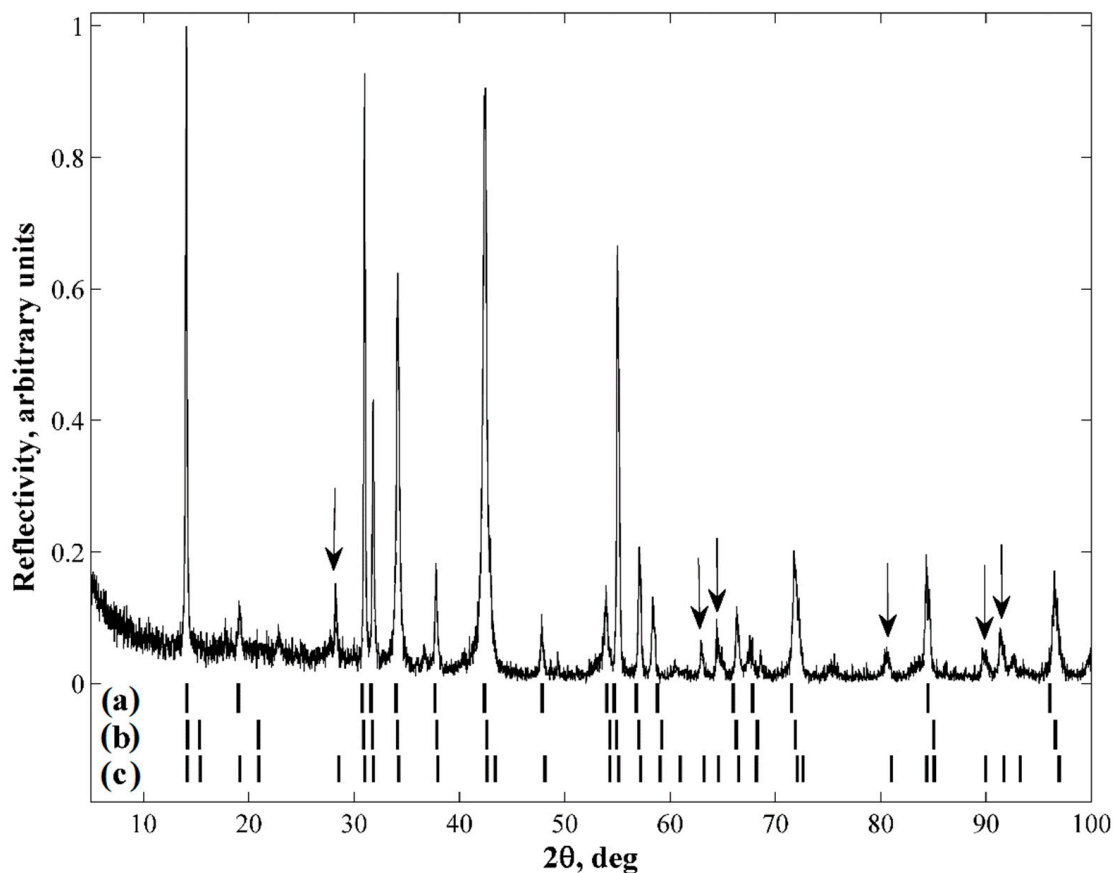


Figure 1. The experimental X-ray diffraction spectrum of $\text{Mn}_{0.30}\text{NbS}_2$ powder and comparison spectra for (a) $\text{Mn}_{0.33}\text{NbS}_2$, crystal superstructure, (b) $\text{Mn}_{0.25}\text{NbS}_2$, crystal superstructure, and (c) $\text{Mn}_{0.30}\text{NbS}_2$ calculated according to the data of single-crystal X-ray diffraction.

4. Magnetic Properties

The temperature dependencies of the dynamic magnetic susceptibility of $\text{Mn}_{0.30}\text{NbS}_2$ single crystal were measured for two different orientations of the crystal in an external magnetic field:

- the magnetic field was in the basal plane ab ($H_{rf} \perp c$);
- the magnetic field was oriented along the hexagonal axis c ($H_{rf} \parallel c$).

In the $H_{rf} \perp c$ orientation, a decrease in the temperature below $T_{C1} = 100$ K leads to an abrupt increase in the susceptibility χ (Figure 2a). A further decrease in the temperature to 50 K leads to a slight decrease in the susceptibility. The second abrupt increase in the magnetic susceptibility χ occurs in the dependence $\chi(T)$ near $T_{C2} = 40$ K. It is obvious that these increases in the magnetic susceptibility are due to the phase transitions to magnetically ordered states.

The application of a constant magnetic field in the basal plane ($H \perp c$) has little effect on the position of the transition temperature T_{C1} ; however, it leads to an abrupt decrease in the dynamic magnetic susceptibility in the temperature range between T_{C1} and T_{C2} . At the same time, the dependence $\chi(T)$ becomes smooth near T_{C2} , and the phase transition expands to a wider temperature range. The external magnetic field up to $H = 150$ Oe has little effect on the magnetic susceptibility χ below the second critical temperature T_{C2} .

In the $H_{rf} \parallel c$ orientation, a phase transition near $T_{C1} = 100$ K is accompanied by only a slight increase in the susceptibility χ (Figure 2b). With a decrease in the temperature from 50 K to $T_{C2} = 40$ K, an abrupt increase in the magnetic susceptibility is observed. Below 40 K, $\chi(T)$ demonstrates nonmonotonic behavior with a minimum near 20 K. The constant

magnetic field applied to the sample does not cause qualitative changes in the dependence $\chi(T)$.

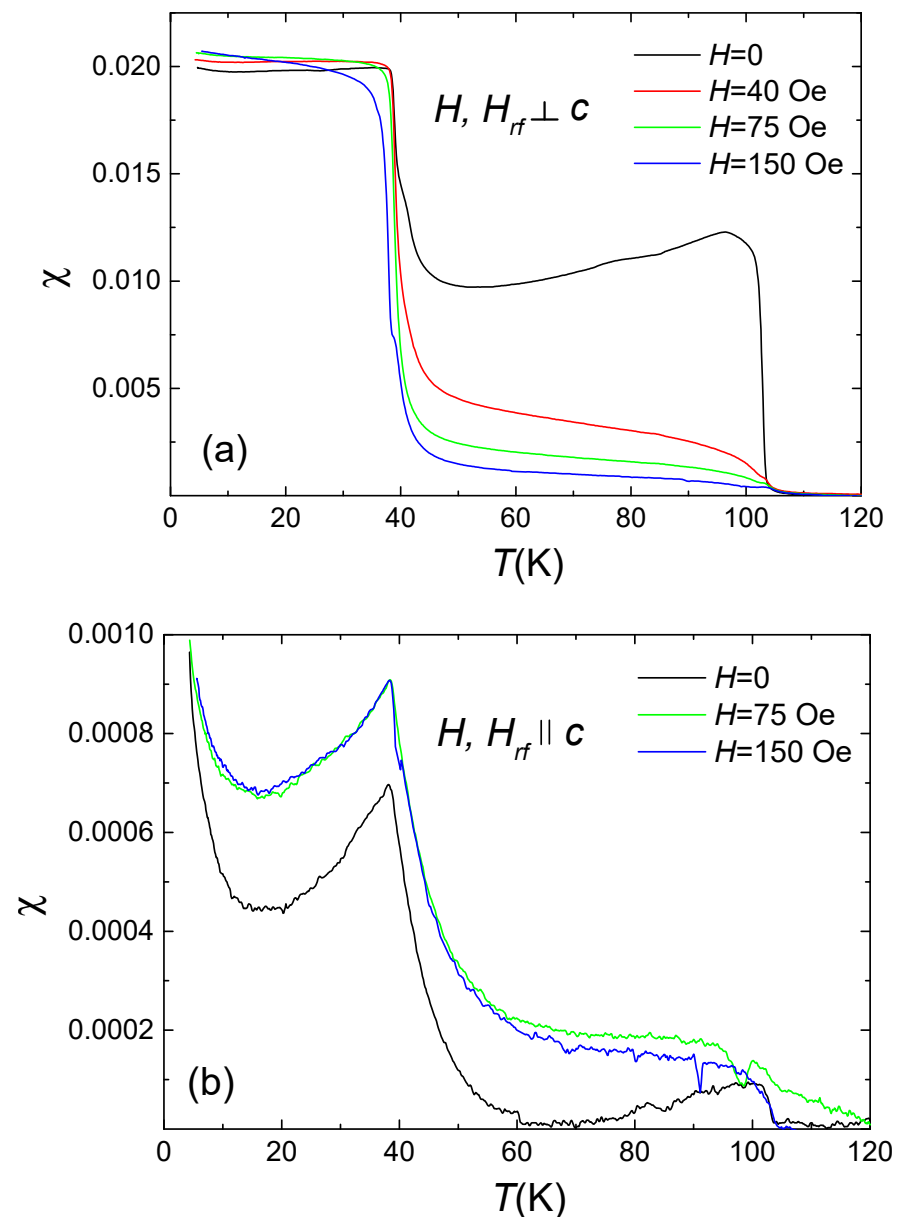


Figure 2. Temperature dependencies of the magnetic susceptibility χ of $\text{Mn}_{0.30}\text{NbS}_2$ single crystals obtained in different magnetic fields in $H \perp c$ (a) and $H \parallel c$ (b) orientations.

Let's consider the first phase transition. At $T_{C1} = 100$ K, an abrupt increase in the magnetic susceptibility in the basal plane and a small change in $\chi(T)$ along the hexagonal axis c occur. This indicates the transition to an anisotropic magnetically ordered ferro- or ferrimagnetic state. Then, a smooth decrease in χ with a temperature decrease below T_{C1} is due to the Hopkinson effect, which is observed in ferro- and ferrimagnetic materials. Below the magnetic ordering temperature T_{C1} , the application of a small ($H = 10$ Oe) constant magnetic field in the basal plane leads to a decrease in the susceptibility by several times. These peculiarities indicate the easiness of magnetic ordering in the basal plane.

Thus, the experimental data indicate that an "easy-plane" ferromagnetic structure is formed at T_{C1} . The critical temperature and the type of magnetic ordering are similar to those observed in the $\text{Mn}_{0.25}\text{NbS}_2$ compound.

The second magnetic phase transition at $T_{C2} = 40$ K is accompanied by an abrupt increase in the magnetic susceptibility both along the hexagonal axis and in the basal plane. Moreover, χ almost does not depend on the applied magnetic field and its direction. This fundamental difference in the dependencies $\chi(H)$ in the basal plane above and below the critical temperature T_{C2} provides evidence of a change in the type of magnetic ordering at this temperature.

The magnetic susceptibility χ in the basal plane is greater than susceptibility along the hexagonal axis both above and below T_{C2} . Consequently, the transition at T_{C2} is not related to a change in the direction of easy magnetization, i.e., the “easy plane”–“easy axis” transition. It is known that a transition to a uniaxial helicoidal state occurs in $\text{Mn}_{0.33}\text{NbS}_2$ at about 40 K. As shown in [35], weak dependencies of susceptibility on the temperature and magnetic field are typical for uniaxial helimagnets away from phase transitions. Although our experimental data do not allow asserting with complete confidence that a magnetic structure formed below T_{C2} is similar to a uniaxial helicoidal phase in $\text{Mn}_{0.33}\text{NbS}_2$, the temperature of the phase transition coinciding within a few degrees and the dependence $\chi(T, H)$ typical for helimagnets are direct evidence for the formation of a helicoidal phase.

Thus, two magnetic phase transitions are observed in the obtained $\text{Mn}_{0.30}\text{NbS}_2$ compound. The first transition is observed at $T_{C1} = 100$ K and corresponds to the transition to an easy-plane ferromagnet phase at $T_{C1} = 100$ K [27,28]. This transition is similar to that in $\text{Mn}_{0.25}\text{NbS}_2$ with the crystal $2a_0 \cdot 2a_0$ superstructure. The second transition is observed at $T_{C2} = 40$ K and is similar to the magnetic ordering of a helicoidal phase in $\text{Mn}_{0.33}\text{NbS}_2$ with the crystal $\sqrt{3}a_0 \cdot \sqrt{3}a_0$ superstructure [17–19].

Two different interpretations of the presence of two critical temperatures in the compound under study can be proposed. On the one hand, in $\text{Mn}_{0.30}\text{NbS}_2$ the aggregation of intercalated Mn ions and the formation of the clusters of $\text{Mn}_{0.33}\text{NbS}_2$ and $\text{Mn}_{0.25}\text{NbS}_2$ phases are possible. In this case, the coexistence of clusters of two different phases in one crystal will result in the presence of two different critical temperatures of magnetic ordering. This interpretation is evidenced by a significant variation in the concentration of Mn ions, $x = 0.30 \pm 0.05$, in the crystals under study.

On the other hand, both temperatures of magnetic ordering may correspond to the same crystallographic phase. This phase is an intermediate superstructure of the $2\sqrt{3}a_0 \cdot 2\sqrt{3}a_0$ type. The compound under consideration has a layered structure, which results in interlayer exchange interactions being significantly weaker than exchange interactions inside one layer. Then, the phase transition at $T_{C1} = 100$ K corresponds to the ferromagnetic ordering of intercalated ions located in the same layer, while the phase transition at $T_{C2} = 40$ K corresponds to interlayer ordering and the formation of a “simple spiral” helicoidal structure. A similar two-step magnetic transition was found earlier in $\text{DyNi}_2\text{B}_2\text{C}$ [36]. The existence of the $2\sqrt{3}a_0 \cdot 2\sqrt{3}a_0$ superstructure is indicated by the presence of additional reflections in the X-ray diffraction spectra, as well as the parameters of the crystal lattice, which differ significantly from those of the $2a_0 \cdot 2a_0$ and $\sqrt{3}a_0 \cdot \sqrt{3}a_0$ superstructures. Moreover, in the $H \perp c$ orientation the experimental dependence $\chi(T)$ (Figure 2a) contradicts the proposed “cluster” interpretation. In the case of the “cluster” origin of the critical temperatures T_{C1} and T_{C2} , the susceptibility χ will be a sum of two terms $\chi_{\text{ferro}} + \chi_{\text{helix}}$. The first term, χ_{ferro} , corresponds to the ferromagnetic phase of $\text{Mn}_{0.25}\text{NbS}_2$ clusters and decreases smoothly with a decrease in the temperature due to the Hopkinson effect. The second term, χ_{helix} , corresponds to the helicoidal phase of $\text{Mn}_{0.33}\text{NbS}_2$ clusters and almost does not depend on the temperature at $T < 40$ K. Then, the resulting susceptibility χ will decrease with a decrease in the temperature both above and below T_{C2} , and the contribution χ_{helix} will lead to the emergence of a peak near $T_{C2} = 40$ K. In our experiments, $\chi(T)$ is almost independent of temperature below 40 K, which indicates the absence of the ferromagnetic contribution χ_{ferro} below T_{C2} . Consequently, the transition of a ferromagnetic phase to a helicoidal phase is observed at T_{C2} .

Thus, the comparison of two critical temperatures T_{C1} and T_{C2} with one crystal $2\sqrt{3}a_0 \cdot 2\sqrt{3}a_0$ superstructure seems to be a more probable explanation of the experimental results.

5. Conclusions

Intercalated $\text{Mn}_{0.30}\text{NbS}_2$ crystal has been obtained. The crystal structure and magnetic properties of this crystal have been studied. The spacing of the crystal structure in the basal plane $a = b = 11.53 \text{ \AA}$ exceeds the spacing of the known $\text{Mn}_{0.33}\text{NbS}_2$ and $\text{Mn}_{0.25}\text{NbS}_2$ compounds by several times. A new type of crystal superstructure $2\sqrt{3}a_0 \cdot 2\sqrt{3}a_0$ is most likely to be formed in the investigated compound; it is an intermediate type between “basic” $2a_0 \cdot 2a_0$ and $\sqrt{3}a_0 \cdot \sqrt{3}a_0$ superstructures. Two critical temperatures are found in the temperature dependence of the dynamic magnetic susceptibility χ . The first critical temperature, $T_{C1} = 100 \text{ K}$, corresponds to the transition from a paramagnetic state to an “easy-plane” ferromagnetic phase. The second critical temperature, $T_{C2} = 40 \text{ K}$, corresponds to the transition to a uniaxial helimagnet phase. Both critical temperatures may correspond to the $2\sqrt{3}a_0 \cdot 2\sqrt{3}a_0$ superstructure and reflect the two-step nature of magnetic ordering. The magnetic ordering of intercalated ions in the basal plane occurs at T_{C1} , and the interlayer ordering with the formation of a helicoidal structure occurs at T_{C2} . We believe that our exciting results are a good motivation for more in-depth studies of intercalated transition metal dichalcogenides near $x = 0.3$, in order to obtain both new material properties and fundamental knowledge. We also would like to emphasize the prospects of the M_xTX_2 series as excellent candidates for assembling van der Waals heterostructures with unusual magnetic properties.

Author Contributions: Conceptualization, methodology, software, validation, formal analysis, investigation, resources, data curation, writing—original draft preparation, visualization, supervision, funding acquisition, F.M., A.S. and D.S.; writing—review and editing, M.P.; project administration, A.S. All authors have read and agreed to the published version of the manuscript.

Funding: This research was funded by Osipyan Institute of Solid State Physics RAS.

Institutional Review Board Statement: Not applicable.

Informed Consent Statement: Not applicable.

Data Availability Statement: Not applicable.

Conflicts of Interest: The authors declare no conflict of interest.

References

1. Radisavljevic, B.; Radenovic, A.; Brivio, J.; Giacometti, V.; Kis, A. Single-layer MoS_2 transistors. *Nat. Nanotechnol.* **2011**, *6*, 147–150. [[CrossRef](#)]
2. Choi, W.; Kim, S. Thin-Film Transistors Based on Transition Metal Dichalcogenides. In *Nanomaterials, Polymers, and Devices: Materials Functionalization and Device Fabrication*; Kong, E.S.W., Ed.; John Wiley & Sons, Inc.: Hoboken, NJ, USA, 2015.
3. Lan, Y.-W.; Torres, C.; Tsai, S.-H.; Zhu, X.; Shi, Y.; Li, Y.; Ming, Y.; Li, L.-J.; Yeh, W.-K.; Wang, K. Atomic-monolayer MoS_2 band-to-band tunneling field-effect transistor. *Small* **2016**, *12*, 5676–5683. [[CrossRef](#)]
4. Tang, L.; Xu, R.; Tan, J.; Yuting, L.; Zou, J.; Zongteng, Z.; Zhang, R.; Zhao, Y.; Lin, J.; Zou, X.; et al. Modulating Electronic Structure of Monolayer Transition Metal Dichalcogenides by Substitutional Nb-Doping. *Adv. Func. Mater.* **2020**, *31*, 2006941. [[CrossRef](#)]
5. Szcześniak, D.; Hoehn, R.D.; Kais, S. Canonical Schottky barrier heights of transition metal dichalcogenide monolayers in contact with a metal. *Phys. Rev. B* **2018**, *97*, 195315. [[CrossRef](#)]
6. Pak, J.; Lee, I.; Cho, K.; Kim, J.-K.; Jeong, H.; Hwang, W.-T.; Ahn, G.; Kang, K.; Yu, W.; Javey, A.; et al. Intrinsic optoelectronic characteristics of MoS_2 phototransistors via a fully transparent van der Waals heterostructure. *ACS Nano* **2019**, *13*, 9638–9646. [[CrossRef](#)]
7. Szcześniak, D.; Kais, S. Gap states and valley-spin filtering in transition metal dichalcogenide monolayers. *Phys. Rev. B* **2020**, *101*, 115423. [[CrossRef](#)]
8. Zhang, J.; Du, C.; Dai, Z.; Chen, W.; Zheng, Y.; Li, B.; Zong, Y.; Wang, X.; Zhu, J.; Yan, Q. NbS_2 nanosheets with M/Se (M = Fe, Co, Ni) codopants for Li^+ and Na^+ storage. *ACS Nano* **2017**, *11*, 10599–10607. [[CrossRef](#)]

9. Zhou, J.; Shen, Y.; Lv, F.; Zhang, W.; Lin, F.; Zhang, W.; Wang, K.; Luo, H.; Wang, Q.; Yang, H.; et al. Ultrathin Metallic NbS₂ Nanosheets with Unusual Intercalation Mechanism for Ultra-Stable Potassium-Ion Storage. *Adv. Funct. Mater.* **2022**, *32*, 2204495. [CrossRef]
10. Splendiani, A.; Sun, L.; Zhang, Y.; Li, T.; Kim, J.; Chim, C.-Y.; Galli, G.; Wang, F. Emerging photoluminescence in monolayer MoS₂. *Nano Lett.* **2010**, *10*, 1271–1275. [CrossRef]
11. Chernenko, A.; Brichkin, A.; Golyshev, G.; Shevchun, A. Effect of the Quality of Interfaces on the Photoluminescence of Encapsulated MoSe₂ Monolayers. *Bull. Russ. Acad. Sci. Phys.* **2023**, *87*, 161–164. [CrossRef]
12. Miyadai, T.; Kikuchi, K.; Kondo, H.; Sakka, S.; Arai, M.; Ishikawa, Y.J. Magnetic properties of Cr_{1/3}NbS₂. *Phys. Soc. Jpn.* **1983**, *52*, 1394–1401. [CrossRef]
13. Koyama, T.; Takayanagi, K.; Mori, S.; Kousaka, Y.; Akimitsu, J.; Nishihara, S.; Inoue, K.; Ovchinnikov, A.S.; Kishine, J. Chiral magnetic soliton lattice on a chiral helimagnet. *Phys. Rev. Lett.* **2012**, *108*, 107202.
14. Ghimire, N.J.; McGuire, M.A.; Parker, D.S.; Sipos, B.; Tang, S.; Yan, J.-Q.; Sales, B.C.; Mandrus, D. Magnetic phase transition in single crystals of the chiral helimagnet Cr_{1/3}NbS₂. *Phys. Rev. B* **2013**, *87*, 104403. [CrossRef]
15. Braam, D.; Tezok, S.; de Mello, E.V.L.; Li, L.; Mandrus, D.; Kee, H.-Y.; Sonier, J.E. Magnetic properties of the helimagnet Cr_{1/3}NbS₂ observed by μ SR. *Phys. Rev. B* **2015**, *91*, 144407. [CrossRef]
16. Sirica, N.; Vilmercati, P.; Bondino, F.; Pis, I.; Nappini, S.; Mo, S.-K.; Fedorov, A.V.; Das, P.K.; Vobornik, I.; Fujii, J.; et al. The nature of ferromagnetism in the chiral helimagnet Cr_{1/3}NbS₂. *Commun. Phys.* **2020**, *3*, 65. [CrossRef]
17. Kousaka, Y.; Nakao, Y.; Kishine, J.; Akita, M.; Inoue, K.; Akimitsu, J. Chiral helimagnetism in T_{1/3}NbS₂ (T= Cr and Mn). *Nucl. Instrum. Methods Phys. Res. A* **2009**, *600*, 250–253. [CrossRef]
18. Karna, S.K.; Womack, F.N.; Chapai, R.; Young, D.P.; Marshall, M.; Xie, W.; Graf, D.; Wu, Y.; Cao, H.; DeBeer-Schmitt, L.; et al. Consequences of magnetic ordering in chiral Mn_{1/3}NbS₂. *Phys. Rev. B* **2019**, *100*, 184413. [CrossRef]
19. Dai, Y.; Liu, W.; Wang, Y.; Pi, L.; Zhang, L.; Zhang, Y.; Fan, J. Critical phenomenon and phase diagram of Mn-intercalated layered MnNb₃S₆. *J. Phys. Condens. Matter* **2019**, *31*, 195803. [CrossRef]
20. Dyadkin, V.; Mushenok, F.; Bosak, A.; Menzel, D.; Grigoriev, S.; Pattison, P.; Chernyshov, D. Structural disorder versus chiral magnetism in Cr_{1/3}NbS₂. *Phys. Rev. B* **2015**, *91*, 184205. [CrossRef]
21. Chen, C.-W.; Chikara, S.; Zapf, V.S.; Morosan, E. Correlations of crystallographic defects and anisotropy with magnetotransport properties in Fe_xTaS₂ single crystals (0.23 ≤ x ≤ 0.35). *Phys. Rev. B* **2016**, *94*, 054406. [CrossRef]
22. Mao, Q.; Xu, Y.; Li, R.; Wang, Y.; Li, H.; Xue, L.; Hao, H.; Khan, R.; Chen, B.; Yang, J. Localized magnetism, magnetic entropy change and critical properties of Mn_{1/4+δ}NbS₂ single crystals. *Phys. B Condens.* **2023**, *649*, 414469. [CrossRef]
23. Anohin, V.Z.; Goncharov, E.G.; Kostjukova, E.P.; Pshestanchik, V.R.; Marshakova, T.A. *Praktikum po Himii i Tehnologii Poluprovodnikov*; M.:Vysshaya shkola: Minsk, Belarus, 1978; p. 191.
24. Inorganic Material Database (AtomWork), National Institute for Materials Science (Japan). Available online: <http://crystdb.nims.go.jp> (accessed on 1 January 2023).
25. Neminsky, A.M.; Nikolaev, P.N.; Shovkun, D.V.; Laukhina, E.E.; Yagubskii, E.B. Temperature dependence of the magnetic field penetration depth in Rb₃C₆₀ measured by ac susceptibility. *Phys. Rev. Lett.* **1994**, *72*, 3092. [CrossRef]
26. Anzenhofer, K.; Van Den Berg, J.M.; Cossee, P.; Helle, J.N. The crystal structure and magnetic susceptibilities of MnNb₃S₆, FeNb₃S₆, CoNb₃S₆ and NiNb₃S₆. *J. Phys. Chem. Solids* **1970**, *31*, 1057–1067. [CrossRef]
27. Blanc-Soreau, A.L.; Rouxel, J.; Gardette, M.; Gorochoy, O. Proprietes electriques et magnetiques de Mn_{0.25}NbS₂ et Mn_{0.33}NbS₂. *Mater. Res. Bull.* **1976**, *11*, 1061–1071. [CrossRef]
28. Rahman, A.; Rehman, M.; Yousaf, M.; Kiani, M.; Zhao, H.; Wang, J.; Lu, Y.; Ruan, K.; Dai, R.; Wang, Z.; et al. RKKY-type in-plane ferromagnetism in layered Mn_{1/4}NbS₂ single crystals. *Phys. Rev. B* **2022**, *105*, 214410. [CrossRef]
29. Hulliger, F.; Pobitschka, E. On the magnetic behavior of new 2H NbS₂-type derivatives. *J. Solid State Chem.* **1970**, *1*, 117–119. [CrossRef]
30. Voorhoeve, J.M.; Berg, V.D.; Robbins, M. Intercalation of the niobium-diselenide layer structure by first-row transition metals. *J. Solid State Chem.* **1970**, *1*, 134–137. [CrossRef]
31. Anzenhofer, K.; de Boer, J.J. The crystal structure of MnNb₄S₈. *Recl. Trav. Chim. Pays-Bas* **1971**, *90*, 56–64. [CrossRef]
32. Onuki, Y.; Ina, K.; Hirai, T.; Komatsubara, T. Magnetic properties of intercalation compound: Mn_{1/4}MX₂. *J. Phys. Soc. Jpn.* **1986**, *55*, 347–356. [CrossRef]
33. Miwa, K.; Ikuta, H.; Hinode, H.; Uchida, T.; Wakihara, M. Synthesis and physical properties of Mn_xNbS₂. *J. Solid State Chem.* **1996**, *125*, 178–181. [CrossRef]
34. Ichikawa, T.; Cho, K. Structural Study of Si (111)(2√3 × 2√3) R30°–Sn Surfaces. *Jpn. J. Appl. Phys.* **2003**, *42*, 5239. [CrossRef]
35. Borich, M.A.; Smagin, V.V.; Tankeev, A.P. Thermodynamics of a helicoidal magnetic structure in a spin-wave approximation. *Phys. Met. Metallogr.* **2014**, *115*, 737–743. [CrossRef]
36. Kuznietz, M.; Takeya, H. Two-step magnetic ordering in as-cast and annealed DyNi₂B₂C samples. *J. Phys. Condens. Matter.* **1999**, *11*, 6561. [CrossRef]

Disclaimer/Publisher’s Note: The statements, opinions and data contained in all publications are solely those of the individual author(s) and contributor(s) and not of MDPI and/or the editor(s). MDPI and/or the editor(s) disclaim responsibility for any injury to people or property resulting from any ideas, methods, instructions or products referred to in the content.